Nano Res (2009) 2: 54–60
DOI 10.1007/s12274-009-9003-1
Research Article

Formation of $Na_{0.44}MnO_2$ Nanowires via Stress-Induced Splitting of Birnessite Nanosheets

Yanguang Li and Yiying Wu (✉)

Department of Chemistry, The Ohio State University, 100 West 18th Avenue, Columbus, Ohio 43210, USA

Received: 1 September 2008 / Revised: 11 November 2008 / Accepted: 12 November 2008

ABSTRACT

High aspect ratio $Na_{0.44}MnO_2$ nanowires with a complex one-dimensional (1–D) tunnel structure have been synthesized. We found that the reaction went through layered birnessite nanosheet intermediates, and that their conversion to the final product involved splitting of the nanosheets into nanowires. Based on our observations, a stress-induced splitting mechanism for conversion of birnessite nanosheets to $Na_{0.44}MnO_2$ nanowires is proposed. The final and intermediate phases show topotaxy with $\langle 001\rangle_f//\langle 020\rangle_b$ or $\langle 110\rangle_b$ where f represents the final $Na_{0.44}MnO_2$ phase and b the intermediate birnessite phase. As a result of their high surface areas, the nanowires are efficient catalysts for the oxidation of pinacyanol chloride dye.

KEYWORDS

Birnessite, manganese oxide, nanowire, nanosheet, stress, conversion

Manganese oxide nanowires with layered or tunnel structures are attractive for applications in batteries, separation and catalysis due to their open-framework structures and interesting redox properties [1–9]. There have been several studies of their synthesis in the literature: for example, MnO_2 nanorods were synthesized through a carefully controlled hydrothermal reaction by oxidizing $MnSO_4$ with $(NH_4)_2S_2O_8$ or $KMnO_4$ [10, 11]. Nanowires with cryptomelane [12], romanechite [6, 13], and RUB –7 [13–15] structures have also been produced in aqueous solution. Most of these approaches involved a birnessite phase observed as an intermediate [11] or used as precursor [6, 13–15]. Birnessite possesses a layered structure formed of edge-sharing MnO_6 octahedra with Na^+ cations and H_2O molecules filling the interlayer space (Fig. 1 (a)). Conversion of birnessite has been used as a general strategy to obtain a variety of tunnel structures [1]. However, the underlying mechanism remains unclear. Recently, the curling or rolling up of birnessite layers as a result of weakened interlayer interactions during hydrothermal treatment was proposed [11]. While this mechanism can explain tube formation from exfoliated molecular sheets, it cannot rationalize the formation of non-hollow manganese oxide nanowires.

Herein we report a stress-induced splitting mechanism that transforms birnessite nanosheets into $Na_{0.44}MnO_2$ nanowires. $Na_{0.44}MnO_2$ has a complex tunnel structure. It consists of columns of edge-sharing MnO_5 square pyramids and sheets of edge-sharing MnO_6 octahedra extending parallel to the *c*-axis (Fig. 1 (b)). They are connected by corner-

Address correspondence to wu@chemistry.ohio-state.edu

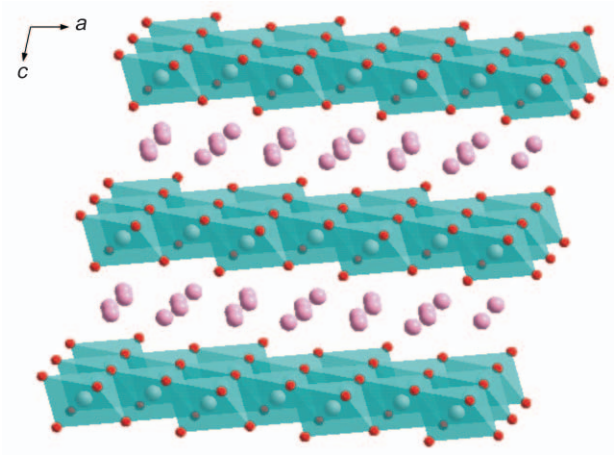

(a)

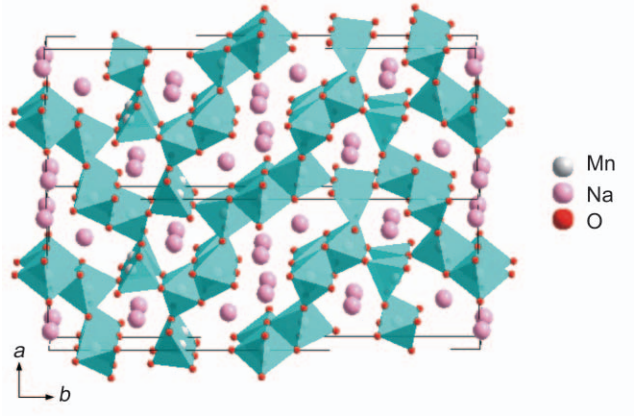

(b)

Figure 1 Schematic illustrations of the crystal structures of birnessite (a) and $Na_{0.44}MnO_2$ (b)

sharing to form two types of tunnels: large S-shaped, and six-sided tunnels, both occupied by Na^+ cations.

In our study, $Na_{0.44}MnO_2$ nanowires were synthesized by a hydrothermal method. Their X-ray diffraction (XRD) pattern shows diffraction peaks in good agreement with the standard pattern (PDF No. 27–0750), except for some variation in peak intensities due to nanowire orientation (Fig. 2(a)). An scanning electron microscopy (SEM) image reveals that they are pure nanowires with average length over 10 μm and diameter smaller than 100 nm (Fig. 2(b)). Most of the nanowires align with each other and form thicker nanowire bundles.

Nanowire growth was tracked at different reaction stages in order to probe their formation mechanism. The birnessite phase appeared first shortly (~2 h) after the start of the reaction as indicated by the XRD pattern of Fig. 3(a)(A). An interlayer spacing of 0.72 nm is calculated from the diffraction peaks at 12.4° and 25.1°, in good agreement with Ref. [16]. The reflection at 15.4°, corresponding to an interlayer spacing of 0.56 nm comes from a dehydrated Na-birnessite phase [16]. The SEM image of the sample at this stage features a large amount of thin nanosheets (see Fig. S-1(a) in the Electronic Supplementary Material (ESM)). Their flat geometry is the cause of the preferred orientation indicated by the abnormally strong (00*l*) peaks of birnessite in Fig. 3(a)(A). Figure 3(b) displays the transmission electron microscopy (TEM) image of a piece of Na-birnessite nanosheet collected at this stage (2 h). The transparency indicates its small thickness.

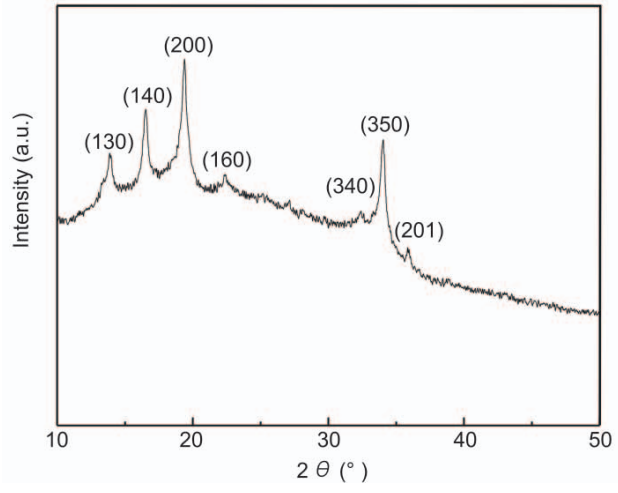

(a)

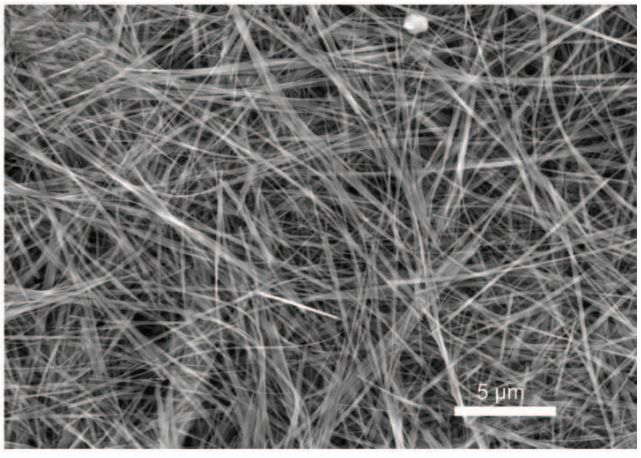

(b)

Figure 2 (a) XRD pattern and (b) SEM image of annealed $Na_{0.44}MnO_2$ nanowires

The corresponding selected area electron diffractions (SAED) pattern shows diffraction spots with roughly six-fold symmetry, and the zone axis is assignable to the [001] axis (Fig. 3(c)). Na-birnessite was reported to be triclinic by Lanson et al. [17, 18]. Its slight deviation from the hexagonal symmetry originates from the elongation along [100] of the Jahn-Teller distorted Mn^{3+} [17, 18]. Close examination of Fig. 3(b) reveals that some nanowires split apart from nanosheets near the edges.

When the reaction time was extended to 2 days, Na-birnessite was still the main phase, together with a significant amount of unreacted Mn_2O_3 and some diffuse peaks from the final product $Na_{0.44}MnO_2$ in the XRD spectrum (Fig. 3(a)(C)). Most of the earlier nanosheets can be seen to have transformed into nanowires in the corresponding SEM image (Fig. S-1(c) in the ESM). Figure 3(d) shows the TEM image of one nanowire collected at this stage. One interesting feature in this nanowire is the thinning from the middle as if it was about to split further (marked by arrows). The corresponding SAED pattern displays elongated lines perpendicular to the nanowire growth direction, in which the original six-fold symmetric diffraction spots are embedded but still visible (marked by triangles in Fig. 3(e)). The striped line features here are a clear indication of transverse structural disorder of the nanowires in the course of conversion from the intermediate birnessite to the final $Na_{0.44}MnO_2$ phase. In contrast, the longitudinal structural order was maintained.

To complete the conversion, reaction for a further two days was found to be necessary. Broad but pronounced peaks of $Na_{0.44}MnO_2$ appear in the XRD pattern (Fig. 3(a)(D)). Figure 3(f) shows a TEM image of the thin nanowires collected at this stage. They

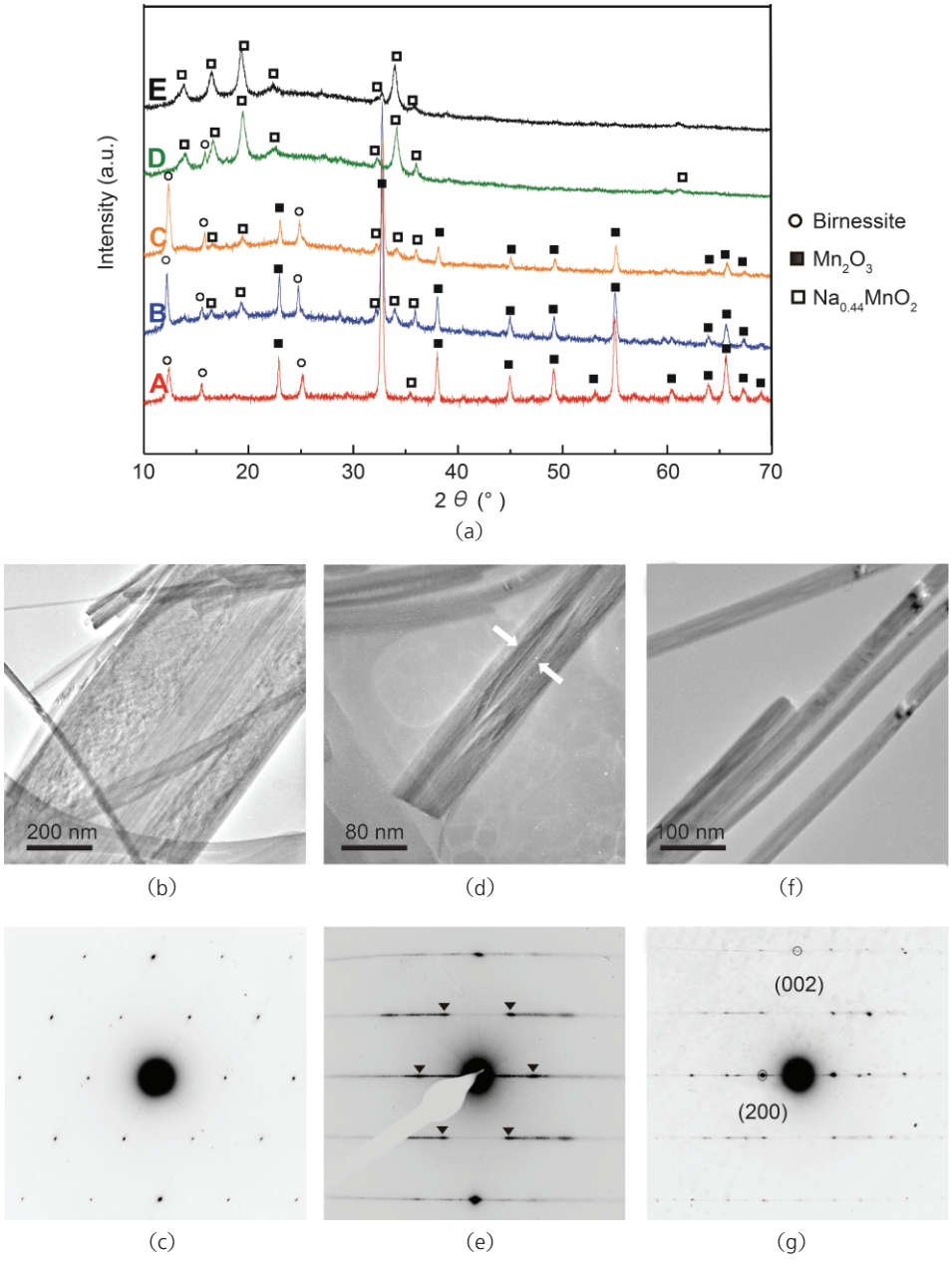

Figure 3 Evolution of $Na_{0.44}MnO_2$ nanowires with time. (a) XRD patterns of the product isolated at different reaction times of (A) 2 h, (B) 24 h, (C) 2 days, (D) 2×2 days, and (E) annealed at 600 °C. TEM and SAED characterizations were also conducted on samples collected at (b), (c) 2 h, (d), (e) 2 days and (f), (g) 2×2 days. The white arrows in (d) indicate nanowire thinning from the middle and the black triangles in (e) mark the six-fold diffraction spots embedded in the elongated lines. In (e) and (g), the nanowires are vertically oriented. See text for detailed discussion

have diameters around 50 nm. A single-nanowire SAED pattern shows diffraction spots of rectangular symmetry (Fig. 3(g)), and nanowire growth direction is determined to be oriented along [002]—the direction of the 1-D tunnel. Similar elongated lines are also present in the background, perpendicular to the nanowire growth direction. We believe these result from defects in the nanowires created during the conversion process.

From the sequence of TEM images, it becomes clear how the birnessite nanosheet intermediates are converted into the $Na_{0.44}MnO_2$ nanowires. The birnessite nanosheets were initially produced by dissolution of Mn_2O_3 powder in concentrated NaOH followed by recrystallization with concomitant intercalation of Na^+ and H_2O. Conversion from the birnessite to various 1-D tunnel structures has been studied for a long time, and is believed to start with a disproportionation reaction of neighboring Mn^{3+} ions in the manganese oxide layers into Mn^{4+} and Mn^{2+} ions [15, 17, 19]. The Mn^{2+} ions migrate into the interlayer galleries, undergo oxidation to Mn^{3+} by oxygen in the autoclave and assist the formation of corner-sharing MnO_6 octahedra. Vacancies left behind weaken the birnessite layers. We believe a similar process occurs in our system. This structural reconstruction introduces a high density of defects, causes stacking faults and in-plane stresses, and eventually the nanosheets split into nanowires when the stress cannot be accommodated any more. This stress-induced splitting mechanism is supported by our observations of the nanowire "brushes" formed after reaction for 2 h. Their overall shape is reminiscent of birnessite nanosheets, as shown by the SEM images in Fig. 4.

Also, noteworthy in Fig. 4 is that the nanowire brushes have two equivalent growth directions with an angle of 60° or 120°. Taken in conjunction with above TEM results, the SEM images suggest that the conversion is topotactic with $\langle 002\rangle_f$ // $\langle 020\rangle_b$ or $\langle 110\rangle_b$ where f represents the final $Na_{0.44}MnO_2$ phase, and b the intermediate birnessite phase. This crystallographic coherence can be understood by comparing the crystal structures of birnessite and the final product. Chains of edge-sharing MnO_6 octahedra run along $\langle 020\rangle$ and $\langle 110\rangle$ in birnessite (Fig. 4(c)). The same feature exists in $Na_{0.44}MnO_2$ along $\langle 002\rangle$. Therefore, $\langle 020\rangle$ and $\langle 110\rangle$ directions are the least stressed during the conversion, and thus the nanosheets tend to split along these directions.

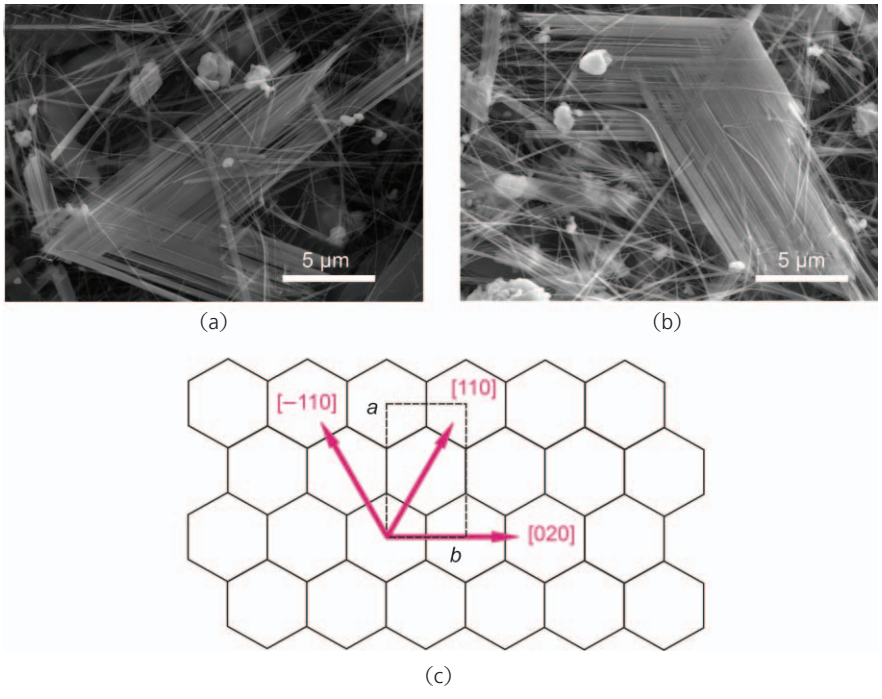

Figure 4 SEM images of nanowire brushes captured at the intermediate stage of the reaction. Their growth is along two directions simultaneously forming an angle of (a) 60° and (b) 120°. (c) Possible nanowire splitting directions in birnessite layers with the edge-sharing MnO_6 octahedra chains preserved. The dashed rectangle represents a 2-D unit cell in the *ab* plane

The proposal of a topotactic conversion is also supported by the similar values of the *d*-spacings (d_{020} = 1.42 Å for birnessite, d_{002} = 1.41 Å for $Na_{0.44}MnO_2$).

To the best of our knowledge, this is the first time that such a mechanism has been proposed for this type of conversion in manganese oxides. We believe it could also apply to other nanowires with tunnel structures synthesized from birnessite [6, 11–13, 15], since it rationalizes some common features observed in such reactions: for example, they all have their one-dimensional tunnels oriented along the nanowires, and they all have similarly small nanowire diameters below 100 nm—possibly a result of reaching a stable size in response to the transverse stress.

We also explored the effect of varying the synthesis conditions. At lower temperatures (for example, 120 °C, see Fig. S-2 in the ESM), birnessite nanosheets are stable against conversion to $Na_{0.44}MnO_2$ nanowires even after reaction for several weeks. With lower NaOH solution concentrations (0.5 –1 mol/L), another type of sodium manganese oxide nanowire with a 2 × 4 tunnel structure is produced (the Na–RUB–7 phase, see Fig. S-3 in the ESM). $Na_{0.44}MnO_2$ could also be ion-exchanged to $Li_{0.44}MnO_2$ by reaction with a molten salt mixture of 88:12 (molar ratio) $LiNO_3$: LiCl at 280 °C for 24 h (Fig. S-4 in the ESM). The nanowire morphology remains intact, and complete Na removal is indicated by the absence of Na peaks in the energ dispersive X-ray (EDX) spectrum.

The catalytic performance of $Na_{0.44}MnO_2$ nanowires for the oxidation of dyes was studied in the presence of H_2O_2. Effluents from the textile industry commonly contain high concentrations of organic dyes, which are potential environmental and health threats if not disposed of properly. An effective and economic approach for their remediation is the catalytic oxidation with H_2O_2 using abundant and nontoxic oxide catalysts, like manganese oxide. Here cationic pinacyanol chloride dye was selected as the prototype to investigate the effectiveness of the $Na_{0.44}MnO_2$ nanowires in the catalytic oxidation of organic dyes [20]. Its UV–vis spectrum shows absorption peaks centered at 600 nm and 545 nm, and a weak shoulder visible around 525 nm (Fig. 5). The peak at 600 nm corresponds to the transition

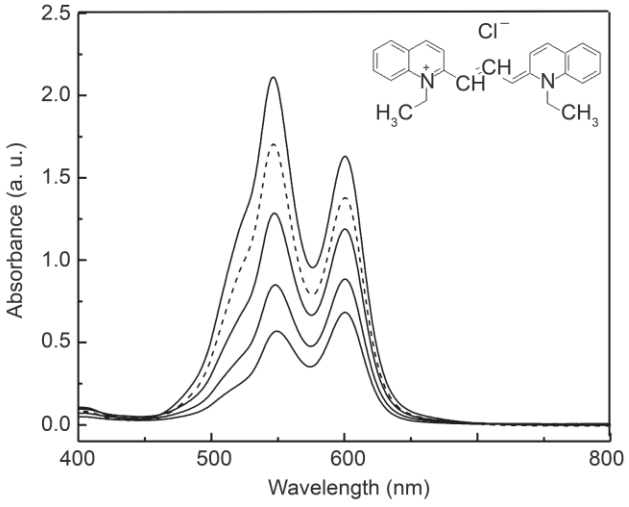

Figure 5 Changes in the visible absorbance spectra of pinacyanol chloride dye during catalytic oxidation by nanowires with H_2O_2. Spectra (solid lines from the top to bottom) were recorded at times of 0, 10, 20, and 30 min, respectively. $Na_{0.44}MnO_2$ powder prepared by a solid state reaction was also tested under the same conditions for comparison; the absorbance spectrum of the dye solution after treatment for 30 min is shown as a dashed line. The insert shows the molecular structure of pinacyanol chloride

between the electronic ground state and the first excited state of the monomer, while the two peaks at shorter wavelength can be assigned to its dimeric form [21]. Stirring a solution of dye and H_2O_2 solution with the nanowires resulted in a continuous decrease in peak intensities. After reaction for 30 min, the peaks at 600 nm and 545 nm were attenuated to 42% and 27% of their original levels, respectively. By contrast, $Na_{0.44}MnO_2$ powder obtained from a solid state reaction [4] showed much poorer reactivity (dashed line). In a control experiment, when no nanowire catalyst was added, the spectrum stayed unchanged after the same reaction period. This indicates the important role of the nanowire catalyst in the oxidative decomposition of the dye, and that any contribution from dye photo-bleaching can be excluded.

It is believed that the oxidative decomposition of the dye proceeds via an adsorption-oxidation-desorption mechanism [20]. Exposed Mn^{3+} and Mn^{4+} ions on the nanowire surface could serve as the active sites for dye adsorption and catalytic centers for the dissociation of H_2O_2 molecules to free radicals such as HO·, HOO· or $O_2^{\cdot-}$[20, 22, 23], which will immediately oxidize dye molecules

in situ. The whole process is surface-limiting and therefore making materials with high surface areas like thin nanowires is beneficial.

In summary, a successful synthesis of $Na_{0.44}MnO_2$ nanowires has been devised. Nanowire growth was found to involve layered birnessite nanosheet intermediates which undergo splitting into nanowires. A stress-induced splitting mechanism is proposed based on our observations. In addition, catalytic oxidation of pinacyanol chloride dye by the nanowires was demonstrated, and their effectiveness comes from their high surface areas.

Methods

To synthesize $Na_{0.44}MnO_2$ nanowires, 0.5 mmol Mn_2O_3 (325 mesh, 99%, Sigma-Aldrich) powder was first mixed with 10 mL of 5 mol/L NaOH (Mallinckrodt) solution and magnetically stirred for 10 min. The suspension was then transferred to a 23 mL autoclave with a Teflon liner (Parr 4749), and heated at 200 °C for two days. The reaction was found to be sensitive to autoclave size and solution filling level, presumably because oxygen in the autoclave participates in the reaction. After reaction for two days, the raw product was repeatedly dispersed in first water and then ethanol, sonicated and then centrifuged to remove most of the NaOH. A second hydrothermal reaction was found necessary to consume all of the Mn_2O_3, and the raw product was mixed again with 10 mL of 5 mol/L NaOH solution and heated at 200 °C for another two days. The resulting product was gel-like, and took the shape of the container. Similar washing steps were adopted as above. Finally, the product was annealed at 600 °C for 2 h with a ramping rate of 1 °C/min to obtain phase-pure $Na_{0.44}MnO_2$ nanowires.

X-ray diffraction patterns were recorded on a Riguka powder diffractometer operating at 40 kV and 25 mA, using Cu Kα radiation. Data were collected with a sampling interval of 0.01°/step and a counting rate of 1 s/step. Scanning electron microscope images and associated energy dispersive spectra were obtained on a Sirion scanning electron microscope, and transmission electron microscope images, high-resolution transmission electron microscope (HRTEM) images and associated selected area electron diffractions (SAED) patterns were recorded on a Tecnai TF-20 instrument.

Oxidative decomposition of pinacyanol chloride dye was carried out at room temperature by dispersing 25 mg nanowires in 50 mL of 10^{-4} mol/L (40 ppm) dye and 5×10^{-4} mol/L H_2O_2 solution. The mixture was allowed to react for 30 min with continuous stirring. UV–vis measurements were conducted on Perkin–Elmer Lambda 950 UV–vis–NIR spectrometer. Small aliquots of the mixture at various time intervals were passed through Millipore 0.2 μm syringe filters (Fisher brand) to remove dispersed nanowires. The solution was diluted 5 times with distilled water prior to the measurement.

Acknowledgements

Yiying Wu acknowledges support from the U.S. Department of Energy under Award No. DE-FG02-07ER46427 and a Research Corporation Cottrell Scholar Award.

Electronic Supplementary Material: SEM studies of nanosheet-to-nanowire conversion, stable Na-birnessite nanosheets synthesized at lower temperature, Na-RUB-7 nanowires synthesized with lower NaOH concentration, and ion-exchanged $Li_{0.44}MnO_2$ nanowires are available in the online version of this article at http://dx.doi.org/10.1007/s12274-009-9003-1 and are accessible free of charge.

References

[1] Feng, Q.; Kanoh, H.; Ooi, K. Manganese oxide porous crystals. *J. Mater. Chem.* **1999**, *9*, 319–333.

[2] Suib, S. L. Microporous manganese oxides. *Curr. Opin. Solid State Mater. Sci.* **1998**, *3*, 63–70.

[3] Suib, S. L. Porous manganese oxide octahedral molecular sieves and octahedral layered materials. *Acc. Chem. Res.* **2008**, *41*, 479–487.

[4] Doeff, M. M.; Anapolsky, A.; Edman, L.; Richardson, T. J.; De Jonghe, L. C. A high-rate manganese oxide for rechargeable lithium battery applications. *J. Electrochem. Soc.* **2001**, *148*, A230–A236.

[5] Hosono, E.; Matsuda, H.; Honma, I.; Fujihara, S.;

Ichihara, M.; Zhou, H. Synthesis of single crystalline electro-conductive $Na_{0.44}MnO_2$ nanowires with high aspect ratio for the fast charge-discharge Li ion battery. *J. Power Sources* **2008**, *182*, 349–352.

[6] Shen, X.; Ding, Y.; Liu, J.; Laubernds, K.; Zerger, R. P.; Polverejan, M.; Son, Y. -C.; Aindow, M.; Suib, S. L. Synthesis, characterization, and catalytic applications of manganese oxide octahedral molecular sieve (OMS) nanowires with a 2 × 3 tunnel structure. *Chem. Mater*. **2004**, *16*, 5327–5335.

[7] Shen, Y. F.; Zerger, R. P.; DeGuzman, R. N.; Suib, S. L.; McCurdy, L.; Potter, D. I.; O'Young, C. L. Manganese oxide octahedral molecular sieves: Preparation, characterization, and applications. *Science* **1993**, *260*, 511–515.

[8] Thackeray, M. M. Manganese oxides for lithium batteries. *Prog. Solid State Chem*. **1997**, *25*, 1–71.

[9] Yuan, J.; Liu, X.; Akbulut, O.; Hu, J.; Suib, S. L.; Kong, J.; Stellacci, F. Superwetting nanowire membranes for selective absorption. *Nat. Nanotechnol*. **2008**, *3*, 332–336.

[10] Wang, X.; Li, Y. Selected-control hydrothermal synthesis of α- and β-MnO_2 single crystal nanowires. *J. Am. Chem. Soc*. **2002**, *124*, 2880–2881.

[11] Wang, X.; Li, Y. Synthesis and formation mechanism of manganese dioxide nanowires/ nanorods. *Chem. -Eur. J*. **2003**, *9*, 300–306.

[12] Portehault, D.; Cassaignon, S.; Baudrin, E.; Jolivet, J. -P. Morphology control of cryptomelane type MnO_2 nanowires by soft chemistry. Growth mechanisms in aqueous medium. *Chem. Mater.* **2007**, *19*, 5410–5417.

[13] Shen, X. -F.; Ding, Y. -S.; Liu, J.; Cai, J.; Laubernds, K.; Zerger, R. P.; Vasiliev, A.; Aindow, M.; Suib, S. L. Control of nanometer-scale tunnel sizes of porous manganese oxide octahedral molecular sieve nanomaterials. *Adv. Mater*. **2005**, *17*, 805–809.

[14] Liu, Z. -H.; Ooi, K. Preparation and alkali-metal ion extraction/insertion reactions with nanofibrous manganese oxide having 2 × 4 tunnel structure. Chem. Mater. **2003**, *15*, 3696_3703.

[15] Xia, G. -G.; Tong, W.; Tolentino, E. N.; Duan, N. -G.; Brock, S. L.; Wang, J. -Y.; Suib, S. L.; Ressler, T. Synthesis and characterization of nanofibrous sodium manganese oxide with a 2 × 4 tunnel structure. *Chem. Mater.* **2001**, *13*, 1585–1592.

[16] Liu, L.; Feng, Q.; Yanagisawa, K.; Wang, Y. Characterization of birnessite-type sodium manganese oxides prepared by hydrothermal reaction process. *J. Mater. Sci. Lett.* **2000**, *19*, 2047–2050.

[17] Lanson, B.; Drits, V. A.; Feng, Q.; Manceau, A. Structure of synthetic Na-birnessite: Evidence for a triclinic one-layer unit cell. *Am. Mineral.* **2002**, *87*, 1662–1671.

[18] Lanson, B.; Drits, V. A.; Silvester, E.; Manceau, A. Structure of H-exchanged hexagonal birnessite and its mechanism of formation from Na-rich monoclinic buserite at low pH. *Am. Mineral.* **2000**, *85*, 826–838.

[19] Silvester, E.; Manceau, A.; Drits, V. A. Structure of synthetic monoclinic Na-rich birnessite and hexagonal birnessite: II. Results from chemical studies and EXAFS spectroscopy. *Am. Mineral.* **1997**, *82*, 962–978.

[20] Segal, S. R.; Suib, S. L.; Foland, L. Decomposition of pinacyanol chloride dye using several manganese oxide catalysts. *Chem. Mater.* **1997**, *9*, 2526–2532.

[21] Sabate, R.; Estelrich, J. Determination of the dimerization constant of pinacyanol: Role of the thermochromic effect. *Spectrochim. Acta A* **2008**, *70*, 471–476.

[22] Thompson, K. M.; Griffith, W. P.; Spiro, M. Mechanism of bleaching by peroxides. Part 3. Kinetics of the bleaching of phenolphthalein by transition-metal salts in high pH peroxide solutions. *J. Chem. Soc., Faraday Trans.* **1994**, *90*, 1105–1114.

[23] Thompson, K. M.; Spiro, M.; Griffith, W. P. Mechanism of bleaching by peroxides. Part 4. Kinetics of bleaching of malvin chloride by hydrogen peroxide at low pH and its catalysis by transition-metal salts. *J. Chem. Soc., Faraday Trans.* **1996**, *92*, 2535–2540.